Single magnetic white dwarfs with Balmer emission lines: a small class with consistent physical characteristics as possible signposts for close-in planetary companions

Boris T. Gänsicke [⬤],[1]★ Pablo Rodríguez-Gil,[2,3] Nicola P. Gentile Fusillo,[4] Keith Inight,[1]
Matthias R. Schreiber,[5,6] Anna F. Pala[4] and Pier-Emmanuel Tremblay[1]

[1]*Department of Physics, University of Warwick, Coventry CV4 7AL, UK*
[2]*Instituto de Astrofísica de Canarias, E-38205 La Laguna, Tenerife, Spain*
[3]*Departamento de Astrofísica, Universidad de La Laguna, E-38206 La Laguna, Tenerife, Spain*
[4]*European Southern Observatory, Karl Schwarzschild Straße 2, D-85748 Garching, Germany*
[5]*Departamento de Física, Universidad Técnica Federico Santa María, Av. España 1680, Valparaíso, Chile*
[6]*Millennium Nucleus for Planet formation, NPF, Av. España 1680, Valparaíso, Chile*

ABSTRACT

We report the identification of SDSS J121929.45+471522.8 as the third apparently isolated magnetic ($B \simeq 18.5 \pm 1.0\,\mathrm{MG}$) white dwarf exhibiting Zeeman-split Balmer emission lines. The star shows coherent variability at optical wavelengths with an amplitude of $\simeq 0.03$ mag and a period of 15.26 h, which we interpret as the spin period of the white dwarf. Modelling the spectral energy distribution and *Gaia* parallax, we derive a white dwarf temperature of $7500 \pm 148\,\mathrm{K}$, a mass of $0.649 \pm 0.022\,\mathrm{M_\odot}$, and a cooling age of 1.5 ± 0.1 Gyr, as well as an upper limit on the temperature of a sub-stellar or giant planet companion of $\simeq 250\,\mathrm{K}$. The physical properties of this white dwarf match very closely those of the other two magnetic white dwarfs showing Balmer emission lines: GD356 and SDSS J125230.93−023417.7. We argue that, considering the growing evidence for planets and planetesimals on close orbits around white dwarfs, the unipolar inductor model provides a plausible scenario to explain the characteristics of this small class of stars. The tight clustering of the three stars in cooling age suggests a common mechanism switching the unipolar inductor on and off. Whereas Lorentz drift naturally limits the lifetime of the inductor phase, the relatively late onset of the line emission along the white dwarf cooling sequence remains unexplained.

Key words: stars: abundances – stars: individual: SDSS J121929.45+471522.8 – planet-star interactions – white dwarfs.

1 INTRODUCTION

White dwarfs are the remnants of stars born with initial masses $\lesssim 8$–$10\,\mathrm{M_\odot}$ (e.g. Smartt et al. 2009; Cummings et al. 2019). Whereas the possibility that some of these stellar remnants possess strong magnetic fields was explored already by Blackett (1947), the observational confirmation occurred only much later (Kemp et al. 1970). It is now firmly established that a small fraction, 2–10 per cent of single white dwarfs exhibit magnetic fields of $B \gtrsim 1\,\mathrm{MG}$ (Ferrario, de Martino & Gänsicke 2015; Hollands, Gänsicke & Koester 2015; Kawka 2020), and there is evidence that weaker fields are equally or possibly even more common (Bagnulo & Landstreet 2019; Landstreet & Bagnulo 2019a, b). The origin of magnetic fields in white dwarfs is still debated, with working hypotheses including fossil fields (Angel, Borra & Landstreet 1981; Braithwaite & Spruit 2004), binary interactions either in the form of a common envelope (Tout et al. 2008, but see Belloni & Schreiber 2020 for a discussion of a number of serious problems in that scenario) or mergers (García-Berro et al. 2012), or processes internal to the white dwarf (Isern et al. 2017).

In the vast majority of magnetic white dwarfs, the presence of the field is established via the detection of Zeeman-split absorption lines of the atmospheric constituents: hydrogen (Angel et al. 1974), helium (Jordan et al. 1998), carbon (Schmidt et al. 1999), and other metals (Kawka & Vennes 2011).

One exception to this rule has been the maverick white dwarf GD356, exhibiting Balmer *emission* lines Zeeman-split in a field of $B \simeq 11\,\mathrm{MG}$ (Greenstein & McCarthy 1985). No binary companion has been detected (Ferrario et al. 1997a), and speculative scenarios explaining the origin of the emission lines included convective activity (Greenstein & McCarthy 1985) or accretion from the interstellar medium (Ferrario et al. 1997a). However, Weisskopf et al. (2007) argued against a hot corona of any kind based on the non-detection of either X-rays or cyclotron radiation. Time-series photometry revealed quasi-sinusoidal variability with an amplitude of 0.2 per cent and a period of $\simeq 115$ min, interpreted as the spin period of the white dwarf (Brinkworth et al. 2004), which is moderately rapid for a single white dwarf (Hermes et al. 2017a).

Left with none of the conventional models providing a satisfactory explanation for the Balmer emission lines, Li, Ferrario & Wickramasinghe (1998) suggested that a conductive planet, or planet core in a close orbit around GD356 would result in the generation of electric currents that could heat the regions near the magnetic poles of the white dwarf – akin to the Jupiter-Io configuration (Goldreich & Lynden-Bell 1969). Wickramasinghe et al. (2010) revisited the unipolar inductor model, arguing that such a planet was unlikely
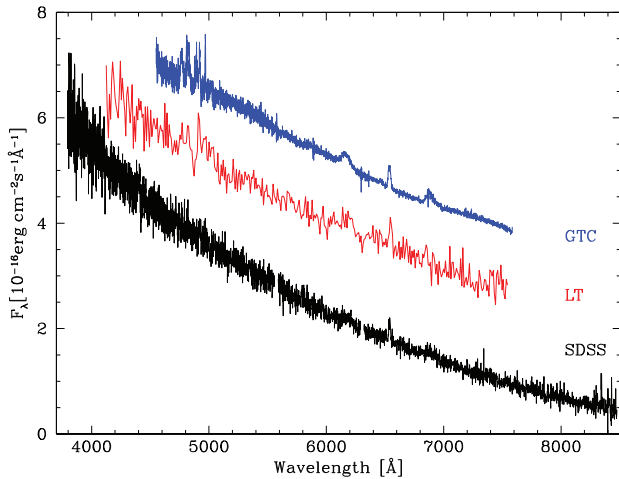
Figure 1. Spectroscopy of SDSS J1219+4715. The SDSS spectrum (2004 April) revealed weak Hα emission, which was confirmed with the LT in 2020 April. Higher resolution spectra obtained with the GTC between 2020 April and June show the Zeeman-split emission lines of Hα and Hβ.

to have survived the giant branch evolution of the progenitor of GD356. Instead, these authors proposed that GD356 is the product of a double-white dwarf merger and the putative planet formed from the metal-rich debris disc left over by this merger (García-Berro et al. 2007) – a rare event, explaining the (at the time) unmatched properties of GD356.

In the light of the rapidly growing evidence for planetesimals and planets around white dwarfs (Becklin et al. 2005; Gänsicke et al. 2006, 2019; Farihi, Jura & Zuckerman 2009; Vanderburg et al. 2015; Manser et al. 2019), Veras & Wolszczan (2019) studied the survivability of conductive planetary cores, and found that a significant parameter space of white dwarf plus planet configurations exists, lending support to the unipolar inductor model.

GD356 remained a fascinating but lonely system for 35 yr, until Reding et al. (2020) announced the discovery of SDSS J125230.93−023417.7 (SDSS J1252−0234), a second magnetic ($B \simeq 5$ MG), single white dwarf exhibiting Zeeman-split Balmer emission lines with an exceptionally short rotation period of 317 s, making it the fastest spinning white dwarf.

We report the identification of a third magnetic ($B \simeq 18.5$ MG), single white dwarf with Zeeman-split Balmer emission lines, SDSS J121929.45+471522.8. We also discuss the physical properties and possible nature of this emerging new class of white dwarfs and their possible link to close planetary companions.

2 OBSERVATIONS

2.1 Spectroscopy

The first spectrum of SDSS J121929.45+471522.8 (SDSS J1219+4715 henceforth) was obtained on 2004 April 21 with the SDSS spectrograph on the 2.5-m SDSS telescope (Fig. 1; York et al. 2000; Adelman-McCarthy et al. 2006), using an exposure time of 2520 s. The SDSS spectrum covers the wavelength range 3800–9200 Å at a spectral resolution of $R = \lambda/\delta\lambda \simeq 1800$. Szkody et al. (2006) noticed a weak Hα emission line in this spectrum and classified SDSS J1219+4715 as a candidate cataclysmic variable (CV), i.e. a short-period interacting binary containing a white dwarf and a low-mass star. The authors argued more specifically that the optical spectrum is likely dominated by

the hot accretion disc of a CV with a relatively high-mass transfer rate. This hypothesis was ruled out by Pala et al. (2020) based on the *Gaia* parallax (Gaia Collaboration 2018), putting the system firmly at a distance of $d = 69.9 \pm 0.6$ pc (Bailer-Jones et al. 2018). Pala et al. (2020) noted that the wavelength of the emission feature is $\simeq 6540$ Å, noticeably blueward of Hα, and tentatively explained it by contamination from the nearby large Seyfert 2 galaxy M 106.

To clarify the nature of SDSS J1219+4715, we obtained one spectrum on 2020 April 21 using the SPectrograph for the Rapid Acquisition of Transients (SPRAT; Piascik et al. 2014) on the robotic Liverpool Telescope (LT; Steele et al. 2004). These data cover the wavelength range $\simeq 4000$–8000 Å with a dispersion of 4.6 Å per pixel, resulting in $R \simeq 340$ at 6000 Å. The exposure time was 1800 s. The SPRAT observations were processed by an automated pipeline which corrects for bias, dark and flat-field effects, performs the sky subtraction and extracts the spectrum, and derives the wavelength and flux calibration. Cosmic rays were manually cleaned from the reduced spectrum. Despite the low resolution, the LT spectrum (Fig. 1) confirmed the emission line near Hα noticed previously in the SDSS spectrum (Szkody et al. 2006). The wavelength of the emission feature is $\simeq 6540$ Å, also blueward of Hα, and within uncertainties identical to that in the SDSS spectrum. Interpreting this line as Doppler-shifted Hα emission would imply a velocity of $\simeq 1000$ km s^{-1}, extremely high for any kind of close white dwarf binary. Moreover, it would be rather unlikely that our LT spectrum sampled the same orbital phase as the SDSS spectrum obtained 16 yr earlier. Closer inspection of the LT spectrum suggested that additional structure was present near Hβ.

Intrigued by the features in the LT spectrum, we acquired higher resolution spectroscopy with the Optical System for Imaging and low-Intermediate-Resolution Integrated Spectroscopy (Sánchez et al. 2012) on the 10.4-m Gran Telescopio Canarias (GTC). The observations were carried out as 600 s exposures in the period April 24 to 2020 June 29. We obtained a total of two and four spectra using the R2500V and R2500R grisms, respectively, which provide $R \simeq 2000$ with the 1-arcsec slit. The wavelengths covered were 4500–6000 Å and 5575–7685 Å for the R2500V and R2500R grisms, respectively.

The GTC spectra were reduced using IRAF.[1] After debiasing and flat-fielding, we performed cosmic ray removal with the L.A.Cosmic package (van Dokkum 2001). Optimal extraction of the spectral trace (Horne 1986) was subsequently done with the STARLINK/PAMELA reduction package (Marsh 1989). We used spectra of HgAr + Ne + Xe arc lamps obtained at the beginning of the nights for wavelength calibration, which was performed with MOLLY.[2]

The GTC spectroscopy reveals that the emission detected previously in the SDSS and LT data is the π component of Zeeman-split Hα emission, flanked to the blue and red by the associated $\sigma^{-,+}$ components (Figs 1 and 2). Multiple sharp emission features are also detected near Hβ, unambiguously identifying SDSS J1219+4715 as a magnetic white dwarf.

2.2 Photometry

Given that many magnetic white dwarfs exhibit photometric variability (Hermes et al. 2017b), we obtained sparse photometry with the robotic LT from 2020 May 19 to 2020 July 6. We used the Bessel *B*-band filter which provides high throughput over the range $\simeq 3800$–4900 Å, covering the higher Balmer lines where photometric

---

[1] IRAF is distributed by the National Optical Astronomy Observatories.
[2] MOLLY is available at http://deneb.astro.warwick.ac.uk/phsaap/software
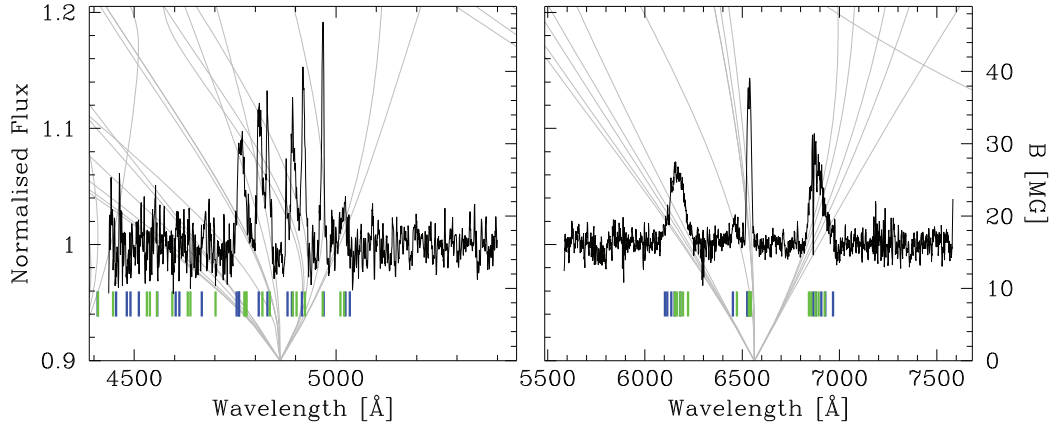
Figure 2. Normalized and averaged GTC spectra of SDSS J1219+4715, centred on Hβ (left) and Hα (right). Shown in grey are the wavelengths of the individual Balmer line components as a function of field strength, which is given on the right-hand side axis. The field strength in SDSS J1219+4715 is near the transition between linear and quadratic Zeeman splitting for Hα, and in the quadratic regime for Hβ. The tick marks below the spectrum indicate the locations of the Balmer transitions in a field of 17.5 MG (green) and 19.5 MG (blue), illustrating that the spread in field strength within the region where the emission lines form is small, $B \simeq 18.5 \pm 1.0$ MG.

variability might be expected. We used the default detector binning of 2×2 and obtained groups of three 80-s exposures separated by at least 2 h. We collected a total of 174 images over 38 individual nights. The LT data are provided in a reduced (bias-corrected and flat-fielded) format, and we extracted the photometry of SDSS J1219+4715 using the pipeline described in Gänsicke et al. (2004) relative to *Gaia* DR2 1545014673992066048 ($G_{BP} = 13.86$), a spectroscopically confirmed G-type star (LAMOST J121936.84+471554.8, Luo et al. 2015, 2019). The photometry revealed SDSS J1219+4715 to be variable with an amplitude of $\simeq 0.03$ mag.

We complemented our LT observations with the *g*- and *r*-band photometry provided by Data Release 3 of the Zwicky Transient Facility (ZTF; Masci et al. 2019), adding 263 observations spanning 2018 April 9 throughout 2019 December 29.

3 ANALYSIS

3.1 Magnetic field

The GTC spectra of SDSS J1219+4715 clearly resolve three components of the Hα emission line (Fig. 2, right-hand panel), which can be identified as the σ^-, π, and σ^+ triplet of Hα within the linear regime of the Zeeman effect, i.e. where the external field removes the energy degeneracy with respect to the magnetic quantum number m_l. However, the different widths of the three components imply that Hα emission originates within an environment with a field strength B where the Zeeman effect transitions into the quadratic regime, removing also the energy degeneracy with respect to the orbital angular momentum l, splitting Hα into 15 transitions (of which two have degenerate energies, hence only 14 components can be observationally be detected, Henry & O'Connell 1985). The GTC spectra reveal a complex structure of multiple sharp emission features of Hβ (Fig. 2, left-hand panel), which transitions into the quadratic Zeeman regime at lower fields compared to Hα. We overplot in Fig. 2 the wavelengths of the individual Hα and Hβ transitions (Friedrich et al. 1996) as a function of B and find that the Hα emission arises in a field of $\simeq 18.5$ MG. Whereas as mentioned above, Hα still largely appears as a linear Zeeman triplet, we do detect the $2p_0 \rightarrow 3s_0$ transition which is split off the other π components.

The Zeeman components of Hα and Hβ shift rapidly as a function of changing B-field, hence any substantial spread in the B-field across the region in which the emission lines arise would smear them out in wavelength. The sharpness of the Hα π components and of the Hβ emission lines implies a homogeneous field within the emitting region. We indicate in Fig. 2 the locations of the individual Zeeman components for $B = 17.5$ MG (green ticks) and $B = 19.5$ MG (blue ticks), and conclude that the Hα and Hβ emission lines arise within a field of $B \simeq 18.5 \pm 1.0$ MG. For a dipolar field structure on the white dwarf, the field near the magnetic equator is a factor 2 lower than the polar field (Achilleos et al. 1992), which implies that the emission lines form in (a) relatively small region(s), most likely near the magnetic pole(s). This is very similar to the situation in GD356, where Greenstein & McCarthy (1985) measured $B = 11 \pm 1.1$ MG in the emitting region and Ferrario et al. (1997a) estimated that this region covers about ten per cent of the white dwarf surface. Similarly, Reding et al. (2020) derived $B = 5.0 \pm 0.1$ MG from the emission lines in SDSS J1252−0234, again implying a small spread in field strength across the region forming the emission lines.

We note that whereas the individual GTC spectra do show some variation in the strength of the Hα emission (Section 3.4), we do not detect photospheric absorption lines from the white dwarf. At a field strength of $\simeq 18.5$ MG, the splitting of the three Zeeman components would by far exceed the pressure-broadening of the Balmer lines, in particular for a white dwarf as cool as SDSS J1215+4715, and hence the photospheric Balmer lines are usually easily visible (see e.g. fig. 9 of Greenstein & McCarthy 1985 and fig. A12 of Tremblay et al. 2020). Most likely, the photospheric absorption lines are filled in by the emission lines and possibly some small amount of continuum flux originating from the same region – which in SDSS J1215+4715 remains visible throughout the spin cycle. We note that in SDSS J1252−0234 the emitting region is self-eclipsed by the white dwarf for parts of the spin cycle, when the emission lines disappear and the photospheric Balmer absorption lines become visible (Reding et al. 2020).

3.2 White dwarf parameters

The standard technique to measure the atmospheric parameters, effective temperature (T_{eff}) and surface gravity (log g), of hydrogen-

Table 1. Stellar parameters of the three magnetic white dwarfs exhibiting Zeeman-split Balmer emission lines.

Parameter		GD356	SDSS J1252−0234	SDSS J1219+4715	References
Parallax	ϖ (mas)	49.65 ± 0.03	12.94 ± 0.11	14.28 ± 0.12	1
Distance	d (pc)	20.1 ± 0.1	77.1 ± 0.7	69.6 ± 0.6	2
Gaia photometry	G (mag)	14.9808 ± 0.0007	17.4775 ± 0.0019	17.5612 ± 0.0018	1
Proper motion	μ_α (mas yr^{-1})	− 119.40 ± 0.06	49.64 ± 0.25	− 113.28 ± 0.11	1
	μ_δ (mas yr^{-1})	− 190.61 ± 0.08	− 39.95 ± 0.16	− 3.492 ± 0.15	1
Effective temperature	$T_{\rm eff}$ (K)	7698 ± 74	7856 ± 101	7500 ± 148	3
Surface gravity	$\log g$ (cgs)	8.22 ± 0.04	7.98 ± 0.06	8.09 ± 0.04	3
Mass	$M_{\rm wd}$ (M$_\odot$)	0.733 ± 0.023	0.583 ± 0.031	0.649 ± 0.022	3
Cooling age	$\tau_{\rm cool}$ (Myr)	1916 ± 144	1136 ± 95	1558 ± 124	3
Magnetic field[a]	B (MG)	11 ± 1.1	5 ± 0.1	18.5 ± 1.0	3, 4, 5
Spin period	P (h)	1.9280 ± 0.0011	0.0881328 ± 0.0000036	15.26415 ± 0.00019	3, 5, 6

Note. (1) Gaia Collaboration (2018); (2) Bailer-Jones et al. (2018); (3) this paper; (4) Greenstein & McCarthy (1985); (5) Reding et al. (2020); (6) Brinkworth et al. (2004), we report the average and standard deviation of their two possible periods. [a]We report the measurements obtained from the emission lines, which correspond to the field strength in the emitting region.

atmosphere white dwarfs from modeling their Stark-broadened Balmer absorption lines (e.g. Bergeron, Saffer & Liebert 1992; Finley, Koester & Basri 1997) is problematic in magnetic white dwarfs, as the simultaneous effect of electric and magnetic fields on the energy levels of hydrogen cannot yet be satisfactorily computed (Jordan 1992; Friedrich et al. 1994). In the case of the three magnetic white dwarfs discussed here, a spectroscopic analysis of their atmospheric parameters is further complicated by the fact that the Balmer emission lines partially or fully fill in the photospheric absorption lines.

None the less, at the moderate magnetic field strengths found at these white dwarfs, the overall spectral energy distribution of a star should not be significantly affected and, given an accurate distance measurement, $T_{\rm eff}$ and $\log g$ can be reliably determined from broadband photometry alone (e.g. Koester, Schulz & Weidemann 1979) when also making use of the well-established mass-radius relation of white dwarfs (Panei, Althaus & Benvenuto 2000; Parsons et al. 2017; Tremblay et al. 2017; Joyce et al. 2018; Chandra et al. 2020). Gentile Fusillo et al. (2019) adopted this method to estimate atmospheric parameters for GD356, SDSS J1252−0234, and SDSS J1219+4715 using the *Gaia* photometry and astrometry, and non-magnetic white dwarf model atmospheres. In the temperature range of these three stars, non-magnetic white dwarfs with hydrogen-rich atmospheres develop convection zones. The effect of magnetic fields on convection has been discussed at length for solar-like stars (e.g. Weiss 1966; Chaplin et al. 2011). In the context of white dwarfs, it has been argued both on theoretical (Tremblay et al. 2015) and observational grounds (Gentile Fusillo et al. 2018) that the presence of fields in excess of $B \simeq 50$–100 kG suppresses convection, which results in an altered temperature structure within the atmosphere compared to weakly- or non-magnetic white dwarfs. For the fields considered here ($B \simeq 5$–18 MG, Table 1), convection will be fully suppressed.

We have therefore re-derived the atmospheric parameters of the three stars fitting non-magnetic, purely radiative model spectra computed by enforcing a convective flux of zero when solving for the atmospheric stratification (Gentile Fusillo et al. 2018). We retrieved *GALEX* (*nuv*; Martin et al. 2005), SDSS (*ugriz*; Albareti et al. 2017) and PanSTARRS (*grizy*; Chambers et al. 2016) photometry for GD356, SDSS J1252−0234, and SDSS J1219+4715 and compared it with synthetic magnitudes calculated from our radiative models, scaled using *Gaia* parallaxes and corrected for reddening using $E(B − V)$ values from the 3D STructuring by Inversion the Local Interstellar Medium reddening map (Lallement et al. 2018). We used a χ^2 minimization routine to find the best-fitting models and

determined the $T_{\rm eff}$ and $\log g$ of the three white dwarfs. As part of this procedure, we noted a marked discrepancy between the observed and predicted photometry in the SDSS-*u* band. This filter covers the wavelength range 3050–4000 Å and is therefore very sensitive to flux changes in the Balmer jump, which are likely to arise from two separate effects. On the one hand, the presence of a magnetic field likely affects the profile of the Balmer jump in a way our models cannot reproduce. On the other hand, it is likely that the region responsible for the emission lines contributes also some small level of continuum flux associated with the bound-free opacity of hydrogen, $\kappa_{\rm bf}$. As $\kappa_{\rm bf} \propto \lambda^3$ up to the ionisation threshold of the considered energy level, this continuum emission is expected to contribute in particular at wavelengths bluewards of the Balmer jump. We therefore decided to exclude the SDSS-*u* band photometry in our final fits.

The atmospheric parameters are reported in Table 1, along with the corresponding white dwarf masses and cooling ages, which we calculated using evolutionary models for thick hydrogen layers.[3] We discuss the interpretation of the cooling ages in the context of the possible evolutionary history of these stars further in Section 4.3. We note that the parameters derived here for SDSS J1252−0234 ($T_{\rm eff} = 7856 \pm 101$ K, $\log g = 7.98 \pm 0.06$) differ somewhat from those of Reding et al. (2020) ($T_{\rm eff} = 8237 \pm 206$ K, $\log g = 8.09 \pm 0.05$), who used convective atmosphere models, and did not make use of the *GALEX nuv* fluxes.

We caution that there is one caveat to the white dwarf parameter determination: additional continuum flux associated with the observed emission lines will affect the fits, most likely resulting (via the scaling factor) in slightly overestimated radii, and hence underestimated masses. SDSS J1252−0234 displays the largest amplitude photometric variability among the three magnetic white dwarfs analysed here ($\simeq 9$ per cent peak-to-peak in a BG40 blue broad bandpass) and is also the only system where the emission lines disappear for a part of the white dwarf spin cycle, suggesting that the emitting region is self-eclipsed behind the white dwarf. Taking nine per cent as a conservative upper limit on the continuum flux contribution (some of the observed photometric variability may be associated with inhomogeneous emission across the surface of the magnetic

---

[3]We use the 2020 version of the cooling models of Holberg & Bergeron (2006), Kowalski & Saumon (2006), Fontaine, Brassard & Bergeron (2001), Tremblay, Bergeron & Gianninas (2011), Bédard et al. (2020) available at http://www.astro.umontreal.ca/~bergeron/CoolingModels.
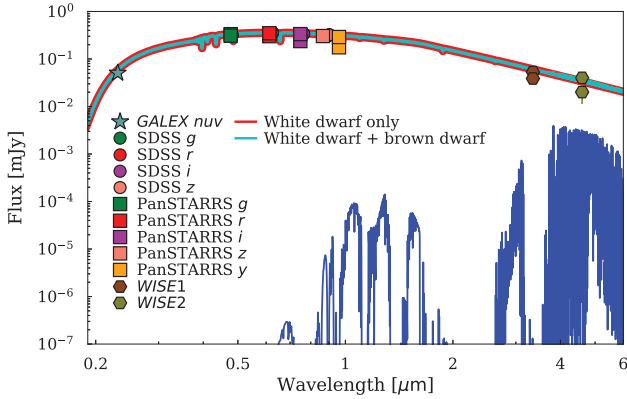
Figure 3. Spectral energy distribution of SDSS J1219+4715 showing the photometry obtained by the different surveys (coloured points). Shown in cyan is a composite model of the best-fitting white dwarf ($T_{\rm eff,wd} = 7500$ K, $\log g = 8.09$, see Section 3.2) and a brown dwarf companion (blue) with effective temperature $T_{\rm eff,bd} \simeq 250$ K, while the red curve shows the white dwarf only.

white dwarfs), our white dwarf radii might be overestimated by three per cent, corresponding to masses underestimated by up to $\simeq 0.028 \, M_\odot$. We note that this is the most extreme case, adopting the largest amplitude observed among the three stars and assuming that it is entirely related to additional emission in excess of the photospheric white dwarf flux. A quantitative assessment of this potential effect will be extremely difficult as it will require high-quality, accurately flux-calibrated, spin-phase resolved spectroscopy, and physically correct models for both the magnetic white dwarf photosphere and the emission region.

3.3 Limits on a possible companion

There is no evidence for a stellar companion at optical wavelengths. To place an upper limit on the presence of a substellar or planetary companion, we complemented the *GALEX* (*nuv*), SDSS (*griz*), and Pan-STARRS (*grizy*) photometry used in Section 3.2 (where we exclude again the SDSS-*u* band for the reasons discussed above) with the *WISE* (*W*1, *W*2) bands (Wright et al. 2010). The reconstructed spectral energy distribution of SDSS J1219+4715 was fitted using a model accounting for both the white dwarf flux and that of a possible low-mass stellar or substellar companion (Fig. 3).

For the white dwarf, we used the best-fitting radiative model spectrum ($T_{\rm eff,wd} = 7500$ K, $\log g = 8.09$, see table 4.1). For the companion, we retrieved a grid of AMES-Cond 2000 models (Allard et al. 2001; Baraffe et al. 2003) for brown dwarfs from the Theoretical Spectra Web Server.[4] The grid covered the range $T_{\rm eff} = 200$–4000 K in steps of 100 K for $Z = Z_\odot$ and a surface gravity $\log g = 4$. The latter was evaluated considering WD 0806−661, a white dwarf with a similar age to SDSS J1219+4715, which has a wide planet-mass companion, $M_{\rm P} = 7 \, M_{\rm J}$ (Luhman, Burgasser & Bochanski 2011). We then assumed a typical radius for the given mass and age, $R = 0.1 \, R_\odot$ (see e.g. fig. 3 from Burrows, Heng & Nampaisarn 2011).

We performed the spectral fit using the Markov chain Monte Carlo implementation for PYTHON, EMCEE (Foreman-Mackey et al. 2013), constraining the white dwarf and the companion to be located at the same distance. The best-fitting model is shown in Fig. 5 (cyan) and implies a brown dwarf companion (blue) with effective temperature

[4]http://svo2.cab.inta-csic.es/theory/newov2/index.php?models=cond00

$T \simeq 250$ K. However, only accounting for the presence of the white dwarf (red) allows to adequately reproduce the observed flux level in the *WISE* filters. Our result thus represents an upper limit on the effective temperature of a possible companion to SDSS J1219+4715.

3.4 Photometric and spectroscopic variability

The combined LT and ZTF light curve of SDSS J1219+4715 extends from 2018 March 25 to 2020 July 6, with a total of 437 photometric epochs. We computed a discrete Fourier transform of the photometry using the TSA context within MIDAS. The resulting amplitude spectrum (Fig. 4, left-hand panel) shows a number of sharp signals spaced out by one-day aliases that are typical of single-site observations. The strongest alias corresponds to a period of $P = 15.26415 \pm 0.00019$ h, where the uncertainty was determined from a sine fit to the data. We subjected the photometric data to a bootstrap test (see Southworth et al. 2006, 2007) and found a 99.9 per cent likelihood that the strongest alias correctly identifies the underlying period. Pre-whitening the light curve with that period and computing a new amplitude spectrum completely removes all significant signals (Fig. 4, left-hand panel).

The limits on the mass and luminosity of a companion to SDSS J1219+4715 (Section 3.3) rule out that the photometric modulation is associated with binarity, and the most likely interpretation is that it reflects the spin period of the white dwarf.

The phase-folded light curve of SDSS J1219+4715 (Fig. 4, right-hand panel) shows a symmetric parabola-shaped minimum that extends in phase, $\Delta\phi \simeq 0.4$. Whereas the ZTF *g*- and *r*-band data, because of their long baseline, are useful in improving the accuracy of the spin period, their photometric precision is insufficient to assess any colour dependence of the modulation.

We established a photometric ephemeris for SDSS J1219+4715 where phase zero corresponds to the minimum brightness of the system,

$$T_0({\rm HJD}) = 2458202.857(1) + 0.6360061(77) \times E. \tag{1}$$

We determined the zero-point by fitting a parabola to the broad minimum in the phase-folded light curve. Using this ephemeris, we computed the phases of the GTC spectra (see Fig. 4, left-hand panel). While our spectroscopic sampling of the spin phase is limited, the data suggest that the strength of the emission lines varies in antiphase with the photometry, i.e. the Hα emission is strongest during the photometric minimum (Fig. 5). We integrated the Hα emission line fluxes after subtracting the underlying continuum using a polynomial fit, and find that the strength of the Hα emission line varies from $(5.2 \pm 0.1) \times 10^{-15}$ erg cm^{-2} s^{-1} near the photometric minimum ($\phi = 0.04$) to $(1.2 \pm 0.1) \times 10^{-15}$ erg cm^{-2} s^{-1} near the photometric maximum ($\phi = 0.57$). Adopting an average Hα flux of 3.2×10^{-15} erg cm^{-2} s^{-1} results in a luminosity of $L({\rm H}\alpha) \simeq 1.9 \times 10^{27}$ erg s^{-1}, which is almost identical to the $\simeq 2 \times 10^{27}$ erg s^{-1} reported by Greenstein & McCarthy (1985) for GD356. Also the emission line flux of Hβ varies in antiphase with the photometric modulation, $(2.8 \pm 0.2) \times 10^{-15}$ erg cm^{-2} s^{-1} at $\phi = 0.06$ and $(1.6 \pm 0.05) \times 10^{-15}$ erg cm^{-2} s^{-1} at $\phi = 0.21$ (the latter spectrum being rather noisy as it was taken under poor conditions). We note that the same antiphased behaviour between the emission lines and the broad-band continuum was observed in SDSS J1252−0234 (Reding et al. 2020) – with the noticeable difference that in this system the emission lines fade completely during the photometric maximum, revealing the photospheric Balmer absorption lines of the white dwarf.

The fact that the emission line fluxes are antiphased with the photometric modulation complicates the interpretation of the latter
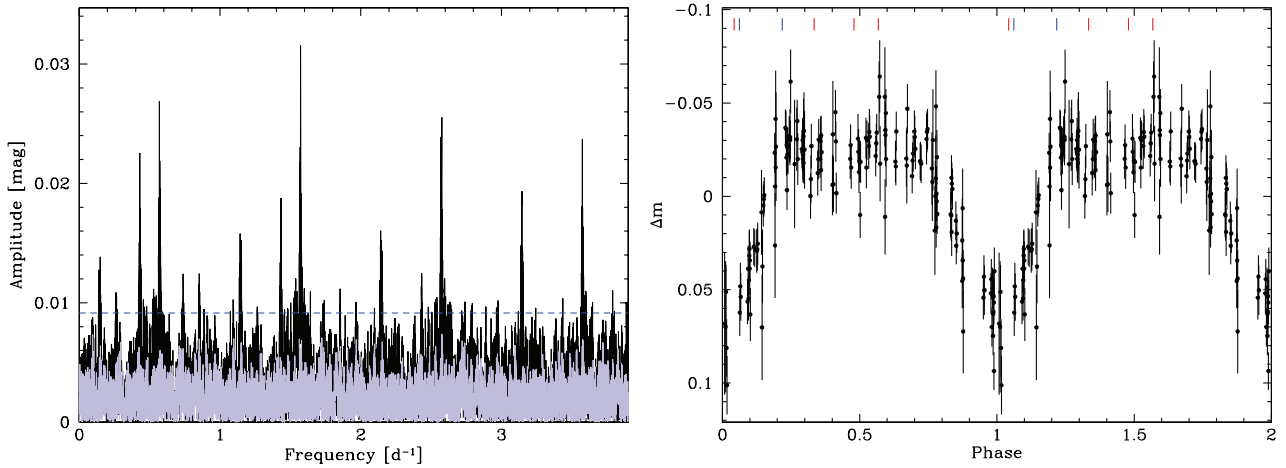
Figure 4. Amplitude spectrum (left-hand panel, computed from the combined ZTF and LT data) and the light curve of SDSS J1219+4715 phase-folded on the 15.26-h period (right-hand panel, LT data only). The red and blue tickmarks above the folded light curve indicate the phases of the H α and H β spectra obtained with the GTC, respectively. The amplitude spectrum (black) shows a complex pattern of aliases, reflecting the window function of the combined ZTF and LT observations. Shown in light blue are the data pre-whitened with a sine wave of $P = 15.26$ h. No signal exceeding the significance threshold (blue dashed line) is detected after the window function is removed.

one, as it is apparently not associated with the additional flux contained in the emission lines. Many single magnetic white dwarfs that do not show Balmer emission lines are known to exhibit spectroscopic and photometric variability as a function of their spin phase (Brinkworth et al. 2005; Euchner et al. 2006; Brinkworth et al. 2013; Hermes et al. 2017b), related to subtle changes in the photospheric spectrum due to the changing viewing geometry of the magnetic field distribution. Accurate, simultaneous spectroscopic (ideally spectropolarimetric) and photometric observations will be required to disentangle the variability intrinsic to the white dwarf and the associated with the emitting region.

4 DISCUSSION

4.1 A closely clustered class of white dwarfs

Inspection of the physical characteristics of GD356, SDSS J1252−0234, and SDSS J1219+4715 (Table 1) and their location in the *Gaia* Hertzsprung–Russell diagram (Fig. 6) shows that they cluster closely in effective temperature ($\simeq 7500$–7860 K), mass ($\simeq 0.58$–$0.73 \, M_\odot$), cooling age ($\simeq 1.1$–1.9 Gyr), and magnetic field strength ($\simeq 5$–19 MG) when compared to the full parameter space occupied by white dwarfs. The tangential velocities of the three stars are $\simeq 20$–$40 \, \mathrm{km \, s^{-1}}$, well within the range of white dwarfs with similar cooling ages (e.g. McCleery et al. 2020), consistent with thin disc membership, and not indicative of any major dynamical interactions in their past lives. A noticeable exception are their spin periods, which span over two orders of magnitude. Non-magnetic single white dwarfs have typical rotation periods of several tens of hours, with very few stars known to spin faster than $\simeq 5$ h (Hermes et al. 2017a). SDSS J1252−0234 is clearly an extreme outlier, requiring an explanation for its very short rotation period (see Section 4.4).

This clustering begs the question: is it representative of an observational selection effect, or reflective of the physical mechanism underlying the still unknown process causing the emission lines? We discuss in Section 4.2 that the spot luminosity is unlikely to be related to ongoing accretion, and we already noticed (Section 3.4) that the
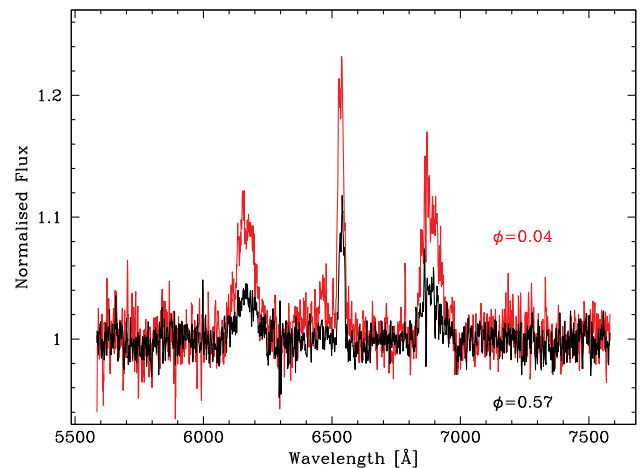
Figure 5. Normalized GTC H α spectra of SDSS J1219+4715 obtained close to the photometric minimum (red) and maximum (black). The strength of the emission lines varies in antiphase with the broad-band photometry, however, the Zeeman components do not shift in wavelength.

strength of the Balmer emission line fluxes in these three stars is similar.

Assuming that these line strengths are typical for the mechanism that produces them, the emission lines would be harder to be detected against the photospheres of hotter, brighter white dwarfs. To simulate this effect, we extracted the H α line fluxes from the GTC average spectrum by subtracting the continuum via a polynomial fit. We then produced a set of DA white dwarf models with $\log g = 8.09$ and temperatures ranging from 6000 to 10 000 K, scaled them to a distance of 69.6 pc, and added Gaussian noise to emulate the data quality of the GTC spectra. Finally, we added the observed emission line fluxes to the (noisy) white dwarf models, and subjected them both to a visual inspection and an equivalent width measurement of the H α region. The conclusion from this exercise was that the H α line fluxes seen in SDSS J1219+4715 would be detectable in white dwarfs with temperatures of up to $\simeq 9000$ K – corresponding to a cooling age of $\simeq 1$ Gyr, or $\simeq 60$ per cent of the present cooling age of SDSS J1219+4715. Assuming that the mechanism that generates
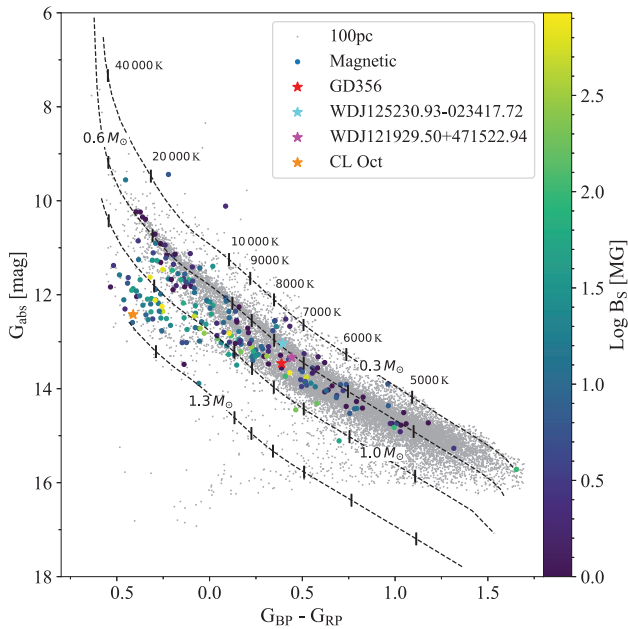
Figure 6. Hertzsprung–Russell diagram of the white dwarfs within 100 pc (Gentile Fusillo et al. 2019), with those known to be magnetic (Ferrario et al. 2015; Hollands et al. 2017; McCleery et al. 2020) colour-coded by their field strength. The three magnetic white dwarfs exhibiting Zeeman-split emission lines cluster extremely closely within the parameter space spanned by the overall population of magnetic white dwarfs. White dwarf cooling tracks[3] for a range of white dwarf masses are superimposed, with temperatures along those tracks indicated as short vertical tick marks. For comparison, the massive ($M_{wd} \simeq 1.3\,M_{\odot}$), rapidly spinning ($P = 725\,$s) and strongly magnetic ($B \simeq 100$–$800\,$MG) white dwarf CL Oct which is discussed as a merger product (Barstow et al. 1995; Ferrario et al. 1997b; Külebi et al. 2010), is shown as an orange star – clearly differing from the three stars discussed here.

the emission lines is always active, there is hence a reasonably long period of time where they could be detected at slightly hotter effective temperatures, and a similar reasoning holds true for the other two systems. It therefore appears somewhat coincidental that all three white dwarfs are found at ages which are clearly past the detection threshold – and there is no shortage of slightly hotter and younger magnetic white dwarfs (Fig. 6).

However, the question of observational selection effects becomes more problematic at lower temperatures – as the white dwarf luminosity decreases, it should be *easier* to detect emission lines of similar strength among cooler magnetic white dwarfs. There is a substantial number of magnetic white dwarfs with $T_{eff} \lesssim 7000\,$K, and emission lines were detected in none of those (Ferrario et al. 2015; Hollands et al. 2015, 2017; Landstreet & Bagnulo 2019b; Kawka 2020; McCleery et al. 2020). It appears hence that the mechanism causing the emission lines in the three stars discussed here is no longer active among cooler magnetic white dwarfs.

Thus, taking the clustering of these three stars at face value suggests that whatever the mechanism responsible for the emission lines is, it becomes active at $T_{eff} \simeq 7700\,$K, and is relatively short-lived, $\simeq 0.5$–$1\,$Gyr. A quick comparison of the rotational kinetic energy of the white dwarfs with the estimated luminosity of the emission lines rules out that the emission process itself results in a sufficiently rapid spin-down of the white dwarf that might eventually stop the mechanism. Within the unipolar inductor model involving a planet in a close-in orbit, the limited lifetime of the planet due to

ohmic dissipation may provide a natural explanation for this short duration (Li et al. 1998; Veras & Wolszczan 2019). However, the late appearance of this effect along the white dwarf cooling track still remains a mystery.

4.2 Origin of the emission lines

The detection of photospheric emission lines from *single* white dwarfs is extremely rare, with the exception of extremely hot and young (pre-) white dwarfs (e.g. Werner 1991; Werner, Heber & Hunger 1991) and a number of helium-atmosphere white dwarfs with $T_{eff} \simeq 14\,000$–$17\,000\,$K (Klein et al. 2020) – in both cases, the presence of the emission lines is intrinsic to their atmospheric structures.

To our knowledge, only the following seven cooler white dwarfs display noticeable emission lines: the three magnetic white dwarfs discussed here (optical Balmer lines, Table 1), one nearby white dwarf with weak, single-peaked Hα emission (McCleery et al. 2020; Tremblay et al. 2020)[5] one white dwarf accreting planetary debris (Ca II H/K lines, PG 1225$-$075, Klein et al. 2010), and two white dwarfs with carbon-dominated (DQ) atmospheres (metal lines in the far-ultraviolet, Provencal, Shipman & MacDonald 2005).

Greenstein & McCarthy (1985) speculated about either chromospheric activity resulting from interactions between convective instabilities and the magnetic field, or accretion causing the emission lines in GD356. Given that the strong magnetic field in GD356 is suppressing convection (Tremblay et al. 2015; Gentile Fusillo et al. 2018), chromospheric activity is unlikely.

Sharp photospheric emission lines are indeed detected among a number of close binaries containing an accreting white dwarf. Examples include several AM CVn systems, ultra-short period binaries consisting of a cool white dwarf accreting from an extremely low-mass degenerate donor (Marsh 1999; Kupfer et al. 2016), and detached white dwarf plus M-dwarf binaries, in which the white dwarf accretes from the stellar wind of its companion (Tappert et al. 2007, 2011). One characteristic that all these systems have in common is that they harbour ($\lesssim 10\,000\,$K) cool white dwarfs that accrete at relatively low rates, and whereas no quantitative model has been developed, it appears likely that it is the energy deposited by the accreted material that results in a temperature inversion in the white dwarf atmosphere, resulting in the observed emission lines.

The system that bears most resemblance to the three magnetic white dwarfs discussed here is SDSS J030308.35+005444.1, a short-period detached binary containing a ($\lesssim 8000\,$K) cool white dwarf plus an M-dwarf (Pyrzas et al. 2009). Parsons et al. (2013) detected Zeeman-split Balmer emission lines, derived a field strength of $\simeq 8\,$MG, and argued that the emission lines are caused by accretion of wind captured by the white dwarf and funnelled towards its magnetic pole(s). A key feature of accretion on to magnetic white dwarfs is that the shock-heated plasma near the white dwarf surface also emits cyclotron radiation (Visvanathan & Wickramasinghe 1979; Woelk & Beuermann 1992). At field strengths of $\sim 10\,$MG, the

---

[5]The sharp Hα emission in WD J041246.85+754942.26 showed no radial velocity variation in observations obtained on three consecutive nights, and the optical-to-infrared spectral energy distribution rules out a companion earlier than a T-type brown dwarf. At the moment, the origin of this emission line remains unexplained, and the association with the stars discussed here is unclear. With $T_{eff} \simeq 8500\,$K, $\log g \simeq 8.25$, WD J0412+7549 lies close to the three magnetic white dwarfs exhibiting Balmer line emission, and one speculative hypothesis is that it might have a weak field ($B \lesssim 100\,$kG). Additional observations of this white dwarf are encouraged.

cyclotron emission lines are located in the near-infrared, and are indeed detected in SDSS J030308.35+005444.1 as an infrared excess over the M-dwarf (Debes et al. 2012).

Given their field strengths of 5–19 MG (Table 1), accretion on to the three single magnetic white dwarfs with Zeeman-split Balmer emission lines should equally result in cyclotron emission, with an associated infrared excess – which is, however, detected in none of them. This strongly argues against ongoing accretion as the cause for the observed emission lines. This extends the conclusions of Weisskopf et al. (2007), who placed an upper limit on the X-ray luminosity of GD356 of $L_x \leq 6 \times 10^{25}\,\mathrm{erg\,s^{-1}}$, and already argued that the non-detection of an infrared excess at GD356 is inconsistent with the possible presence of a hot corona as a source of the Balmer emission lines (see also Musielak, Porter & Davis 1995 for an earlier X-ray study of GD356 and Ferrario et al. 1997a for an additional discussion arguing against ongoing accretion). No X-ray observations of the other two stars discussed here are available.

With both chromospheric activity and accretion being unlikely to be the cause for the Balmer emission lines in these three magnetic white dwarfs, the unipolar inductor model (Li et al. 1998; Wickramasinghe et al. 2010) remains currently the only plausible explanation. This model requires a conductive planet or planet core in a close orbit around each of the three stars, which, in the light of the detections of solid planetesimals (Vanderburg et al. 2015; Manser et al. 2019; Vanderbosch et al. 2020) as well as giant planets (Gänsicke et al. 2019), appears entirely feasible. The fact that all three stars discussed here are relatively nearby ($d \lesssim 80\,\mathrm{pc}$) implies that such configurations of evolved planetary systems may not be exceedingly rare.

4.3 A double-degenerate merger origin?

Wickramasinghe et al. (2010) and Reding et al. (2020) argued that GD356 and SDSS J1252−0234 could originate from double-degenerate mergers, which would explain both the magnetic field and the short rotation periods of their white dwarfs. In addition, second-generation planets may form out of the metal-rich debris disc left behind by the merger event (García-Berro et al. 2007), providing the key component for the unipolar inductor model of Li et al. (1998).

The masses of the three magnetic white dwarfs showing Balmer emission lines, even when accounting for the fact that we may slightly underestimate them (Section 3.2), are close to the average mass of the field white dwarf population,[6] $\langle M_{wd} \rangle \simeq 0.65\,\mathrm{M_\odot}$ (Giammichele, Bergeron & Dufour 2012; Hollands et al. 2018; Tremblay et al. 2020), and hence if produced by double-degenerate mergers, the progenitor binaries would have contained two He-core white dwarfs. Detailed hydro-dynamical simulations of double-degenerate mergers show that He-core mergers eject very little mass ($\lesssim 2 \times 10^{-3}\,\mathrm{M_\odot}$). This implies that the total masses of the double-degenerates that merged were very close to the masses measured for the three magnetic white dwarfs, i.e. $\simeq 0.58$–$0.73\,\mathrm{M_\odot}$.

Inspecting the roster of double-degenerates with measured masses for both components (Breedt et al. 2017; Rebassa-Mansergas et al. 2017; Napiwotzki et al. 2020) suggests that potential progenitor systems matching the top-end of the mass range spanned by the three magnetic systems are known, but that they are rare – and their

merger time-scales are typically exceeding a Hubble time (Geier et al. 2010). Given the large observational bias favouring the identification of lower mass white dwarfs (because of their larger radii), the scarcity of progenitors is exacerbated. We note that progenitors containing one extremely low mass (ELM) white dwarf are even less likely, as the total masses of the known ELM binaries peak[7] at $\simeq 1\,\mathrm{M_\odot}$ (Brown et al. 2016), and as ELM binaries are intrinsically rare (Kawka et al. 2020).

One additional potential issue with invoking second-generation planets forming out of the ejected material is that García-Berro et al. (2007) modelled a $CO + He$ merger. It is not clear if a $He + He$ merger would result in sufficiently metal-rich ejecta to form a conductive, second-generation planet.

Assuming nevertheless a merger origin for these three magnetic white dwarfs, the characteristics of the known population of double-degenerates would suggest that a larger number of similar systems with resulting masses for the merger product of $\simeq 0.8$–$1.0\,\mathrm{M_\odot}$ should exist – yet none has been found so far. Moreover, it would appear very coincidental that these three stars share many of their properties, in particular their effective temperatures and cooling ages, as discussed in the previous section. A double-degenerate merger will result in a re-heated and possibly strongly magnetic white dwarf (García-Berro et al. 2012; Wegg & Phinney 2012), such as it may be the case for CL Oct (see fig. 6, Ferrario et al. 1997b). If the Balmer line mechanism in such a system is active, it should be detectable before it cools down to $\simeq 7700\,\mathrm{K}$ (Section 4.1 and Fig. 6).

We conclude that while a double-degenerate merger origin cannot be ruled out, the clustered properties of these three magnetic white dwarfs and the sufficiently disparate characteristics of the known double-degenerates argue against it. One final note concerns the cooling ages calculated in Section 3.2. In the case of a double-degenerate evolution history, these would approximate the time since the merger event (Wegg & Phinney 2012; Temmink et al. 2020), but that would change none of our arguments regarding the tight clustering of the three stars in their physical properties outlined above and in Section 4.1.

4.4 White dwarf spin-up via accretion from a giant planet?

Our argument against double-degenerate mergers leaves us with the question: how can some single white dwarfs reach very short periods, such as SDSS J1252−0234? A possible answer is, again, linked to planets surviving and scattering into close-in orbits around the white dwarf. Stephan et al. (2020) demonstrated that ingestion of a giant planet can spin-up white dwarfs to close to break-up, thus reaching spin periods in the range of minutes appears entirely possible. The discovery of a giant planet at WD J091405.30+191412.25 (Gänsicke et al. 2019) corroborates that this is a plausible scenario – moreover, if only the gaseous envelope of the giant planet is accreted, but its (conductive) core survives, it naturally provides the key ingredient for the unipolar inductor model.

5 CONCLUSIONS

We have identified SDSS J1219+4715 as an additional magnetic white dwarf exhibiting Zeeman-split Balmer emission lines and photometric variability with a 15.26-h period, which we interpret as being related to the white dwarf rotation. The upper limit on the temperature of a possible substellar or giant planet companion

---

[6]The average white dwarf mass in a magnitude-limited sample is slightly lower, $< M_{wd} > \simeq 0.6\,\mathrm{M_\odot}$, as lower mass white dwarfs are larger and hence can be detected out to larger distances (Koester et al. 1979; Bergeron et al. 1992, 2019; Tremblay et al. 2019).

[7]Exceptions exist, but are *extremely* rare (Brown et al. 2020).

is $\simeq 250$ K. The emission lines originate in a region with a fairly homogeneous field strength of $B \simeq 18.5 \pm 1.0$ MG. Whereas the emission lines vary in flux over the white dwarf spin phase by a factor approximately four, they always remain visible, indicating that the emitting region never fully disappears behind the limb of the white dwarf. With a temperature of 7500 ± 148 K, a mass of $0.649 \pm 0.022 \, M_\odot$, and a cooling age of 1.5 ± 0.1 Gyr, SDSS J1219+4715 very closely resembles the other two members of this small class of stars: GD356 and SDSS J1252−0234. We argue that this clustering in physical parameters, including the strength of the emission line fluxes, suggests a common mechanism that (a) becomes active at cooling ages of $\simeq 1.5$ Gyr, (b) lasts $\simeq 0.5$–1.0 Gyr, and (c) does not affect all magnetic white dwarfs. Given the growing observational evidence for the existence of planetesimals and planets in close orbits around white dwarfs, the unipolar inductor model developed for GD356 seems a plausible scenario that satisfies (b) and (c) above, however, the onset of the emission lines at advanced cooling ages remains unexplained. We encourage closer spectroscopic scrutiny of the known magnetic white dwarfs with temperatures 6000–9000 K to either detect additional examples of this class of stars, or to place stringent upper limits on the presence of Balmer emission lines.

DATA AVAILABILITY

All observational data used in this paper will be available from the public data archives of the SDSS, LT, GTC, and ZTF.

REFERENCES

Achilleos N., Wickramasinghe D. T., Liebert J., Saffer R. A., Grauer A. D., 1992, ApJ, 396, 273
Adelman-McCarthy J. K. et al., 2006, ApJS, 162, 38
Albareti F. D. et al., 2017, ApJS, 233, 25
Allard F., Hauschildt P. H., Alexander D. R., Tamanai A., Schweitzer A., 2001, ApJ, 556, 357
Angel J. R. P., Borra E. F., Landstreet J. D., 1981, ApJS, 45, 457
Angel J. R. P., Carswell R. F., Beaver E. A., Harms R., Strittmatter P. A., 1974, ApJ, 194, L47
Bagnulo S., Landstreet J. D., 2019, A&A, 630, A65
Bailer-Jones C. A. L., Rybizki J., Fouesneau M., Mantelet G., Andrae R., 2018, AJ, 156, 58

Baraffe I., Chabrier G., Barman T. S., Allard F., Hauschildt P. H., 2003, A&A, 402, 701

Barstow M. A., Jordan S., O'Donoghue D., Burleigh M. R., Napiwotzki R., Harrop-Allin M. K., 1995, MNRAS, 277, 971

Becklin E. E., Farihi J., Jura M., Song I., Weinberger A. J., Zuckerman B., 2005, ApJ, 632, L119

Belloni D., Schreiber M. R., 2020, MNRAS, 492, 1523

Bergeron P., Dufour P., Fontaine G., Coutu S., Blouin S., Genest-Beaulieu C., Bédard A., Rolland B., 2019, ApJ, 876, 67

Bergeron P., Saffer R. A., Liebert J., 1992, ApJ, 394, 228

Blackett P. M. S., 1947, Nature, 159, 658

Braithwaite J., Spruit H. C., 2004, Nature, 431, 819

Breedt E. et al., 2017, MNRAS, 468, 2910

Brinkworth C. S., Burleigh M. R., Lawrie K., Marsh T. R., Knigge C., 2013, ApJ, 773, 47

Brinkworth C. S., Burleigh M. R., Wynn G. A., Marsh T. R., 2004, MNRAS, 348, L33

Brinkworth C. S., Marsh T. R., Morales-Rueda L., Maxted P. F. L., Burleigh M. R., Good S. A., 2005, MNRAS, 357, 333

Brown W. R., Gianninas A., Kilic M., Kenyon S. J., Allende Prieto C., 2016, ApJ, 818, 155

Brown W. R., Kilic M., Bédard A., Kosakowski A., Bergeron P., 2020, ApJ, 892, L35

Burrows A., Heng K., Nampaisarn T., 2011, ApJ, 736, 47

Bédard A. et al., 2020, ApJ, 901, 93

Chambers K. C. et al., 2016, preprint (arXiv:1612.05560)

Chandra V., Hwang H.-C., Zakamska N. L., Cheng S., 2020, ApJ, 899, 146

Chaplin W. J. et al., 2011, Science, 332, 213

Cummings J. D., Kalirai J. S., Choi J., Georgy C., Tremblay P.-E., Ramirez-Ruiz E., 2019, ApJ, 871, L18

Debes J. H., Hoard D. W., Farihi J., Wachter S., Leisawitz D. T., Cohen M., 2012, ApJ, 759, 37

Euchner F., Jordan S., Beuermann K., Reinsch K., Gänsicke B. T., 2006, A&A, 451, 671

Farihi J., Jura M., Zuckerman B., 2009, ApJ, 694, 805

Ferrario L., de Martino D., Gänsicke B. T., 2015, Space Sci. Rev., 191, 111

Ferrario L., Vennes S., Wickramasinghe D. T., Bailey J. A., Christian D. J., 1997b, MNRAS, 292, 205

Ferrario L., Wickramasinghe D. T., Liebert J., Schmidt G. D., Bieging J. H., 1997a, MNRAS, 289, 105

Finley D. S., Koester D., Basri G., 1997, ApJ, 488, 375

Fontaine G., Brassard P., Bergeron P., 2001, PASP, 113, 409

Foreman-Mackey D., Hogg D. W., Lang D., Goodman J., 2013, PASP, 125, 306

Friedrich S., Ostreicher R., Ruder H., Zeller G., 1994, A&A, 282, 179

Friedrich S. et al., 1996, A&A, 306, 860

Gaia Collaboration, 2018, A&A, 616, A1

García-Berro E., Lorén-Aguilar P., Pedemonte A. G., Isern J., Bergeron P., Dufour P., Brassard P., 2007, ApJ, 661, L179

García-Berro E. et al., 2012, ApJ, 749, 25

Geier S., Heber U., Kupfer T., Napiwotzki R., 2010, A&A, 515, A37

Gentile Fusillo N. P., Tremblay P.-E., Jordan S., Gänsicke B. T., Kalirai J. S., Cummings J., 2018, MNRAS, 473, 3693

Gentile Fusillo N. P. et al., 2019, MNRAS, 482, 4570

Giammichele N., Bergeron P., Dufour P., 2012, ApJS, 199, 29

Goldreich P., Lynden-Bell D., 1969, ApJ, 156, 59

Greenstein J. L., McCarthy J. K., 1985, ApJ, 289, 732

Gänsicke B. T., Araujo-Betancor S., Hagen H.-J., Harlaftis E. T., Kitsionas S., Dreizler S., Engels D., 2004, A&A, 418, 265

Gänsicke B. T., Marsh T. R., Southworth J., Rebassa-Mansergas A., 2006, Science, 314, 1908

Gänsicke B. T., Schreiber M. R., Toloza O., Fusillo N. P. G., Koester D., Manser C. J., 2019, Nature, 576, 61

Henry R. J. W., O'Connell R. F., 1985, PASP, 97, 333

Hermes J. J., Gänsicke B. T., Gentile Fusillo N. P., Raddi R., Hollands M. A., Dennihy E., Fuchs J. T., Redfield S., 2017b, MNRAS, 468, 1946

Hermes J. J. et al., 2017a, ApJS, 232, 23

Holberg J. B., Bergeron P., 2006, AJ, 132, 1221

Hollands M. A., Gänsicke B. T., Koester D., 2015, MNRAS, 450, 681

Hollands M. A., Koester D., Alekseev V., Herbert E. L., Gänsicke B. T., 2017, MNRAS, 467, 4970

Hollands M. A., Tremblay P.-E., Gänsicke B. T., Gentile-Fusillo N. P., Toonen S., 2018, MNRAS, 480, 3942

Horne K., 1986, PASP, 98, 609

Isern J., García-Berro E., Külebi B., Lorén-Aguilar P., 2017, ApJ, 836, L28

Jordan S., 1992, A&A, 265, 570

Jordan S., Schmelcher P., Becken W., Schweizer W., 1998, A&A, 336, L33

Joyce S. R. G., Barstow M. A., Casewell S. L., Burleigh M. R., Holberg J. B., Bond H. E., 2018, MNRAS, 479, 1612

Kawka A., 2020, preprint (arXiv:2001.10672)

Kawka A., Simpson J. D., Vennes S., Bessell M. S., Da Costa G. S., Marino A. F., Murphy S. J., 2020, MNRAS, 495, L129

Kawka A., Vennes S., 2011, A&A, 532, A7

Kemp J. C., Swedlund J. B., Landstreet J. D., Angel J. R. P., 1970, ApJ, 161, L77

Klein B., Jura M., Koester D., Zuckerman B., Melis C., 2010, ApJ, 709, 950

Klein B. et al., 2020, ApJ, 900, 2

Koester D., Schulz H., Weidemann V., 1979, A&A, 76, 262

Kowalski P. M., Saumon D., 2006, ApJ, 651, L137

Kupfer T., Steeghs D., Groot P. J., Marsh T. R., Nelemans G., Roelofs G. H. A., 2016, MNRAS, 457, 1828

Külebi B., Jordan S., Nelan E., Bastian U., Altmann M., 2010, A&A, 524, A36

Lallement R. et al., 2018, A&A, 616, A132

Landstreet J. D., Bagnulo S., 2019a, A&A, 623, A46

Landstreet J. D., Bagnulo S., 2019b, A&A, 628, A1

Li J., Ferrario L., Wickramasinghe D., 1998, ApJ, 503, L151

Luhman K. L., Burgasser A. J., Bochanski J. J., 2011, ApJ, 730, L9

Luo A.-L., Zhao Y. H., Zhao G., et al., 2019, VizieR Online Data Catalog, V/164

Luo A.-L. et al., 2015, Res. Astron. Astrophys., 15, 1095

Manser C. J. et al., 2019, Science, 364, 66

Marsh T. R., 1989, PASP, 101, 1032

Marsh T. R., 1999, MNRAS, 304, 443

Martin D. C. et al., 2005, ApJ, 619, L1

Masci F. J. et al., 2019, PASP, 131, 018003

McCleery J. et al., 2020, MNRAS, in press, preprint (arXiv:2006.00874)

Musielak Z. E., Porter J. G., Davis J. M., 1995, ApJ, 453, L33

Napiwotzki R. et al., 2020, A&A, 638, A131

Pala A. F. et al., 2020, MNRAS, 494, 3799

Panei J. A., Althaus L. G., Benvenuto O. G., 2000, A&A, 353, 970

Parsons S. G., Marsh T. R., Gänsicke B. T., Schreiber M. R., Bours M. C. P., Dhillon V. S., Littlefair S. P., 2013, MNRAS, 436, 241

Parsons S. G. et al., 2017, MNRAS, 470, 4473

Piascik A. S., Steele I. A., Bates S. D., Mottram C. J., Smith R. J., Barnsley R. M., Bolton B., 2014, in Proc. SPIE Conf. Ser. Vol. 9147. SPIE, Bellingham, p. 91478H

Provencal J. L., Shipman H. L., MacDonald J., 2005, ApJ, 627, 418

Pyrzas S. et al., 2009, MNRAS, 394, 978

Rebassa-Mansergas A., Parsons S. G., García-Berro E., Gänsicke B. T., Schreiber M. R., Rybicka M., Koester D., 2017, MNRAS, 466, 1575

Reding J. S., Hermes J. J., Vanderbosch Z., Dennihy E., Kaiser B. C., Mace C. B., Dunlap B. H., Clemens J. C., 2020, ApJ, 894, 19

Schmidt G. D., Liebert J., Harris H. C., Dahn C. C., Leggett S. K., 1999, ApJ, 512, 916

Smartt S. J., Eldridge J. J., Crockett R. M., Maund J. R., 2009, MNRAS, 395, 1409

Southworth J., Gänsicke B. T., Marsh T. R., de Martino D., Hakala P., Littlefair S., Rodríguez-Gil P., Szkody P., 2006, MNRAS, 373, 687

Southworth J., Marsh T. R., Gänsicke B. T., Aungwerojwit A., Hakala P., de Martino D., Lehto H., 2007, MNRAS, 382, 1145

Steele I. A. et al., 2004, in Oschmann J. M., ed., Proc. SPIE Conf. Ser. Vol. 5489, Ground-based Telescopes. SPIE, Bellingham, p. 679

Stephan A. P., Naoz S., Gaudi B. S., Salas J. M., 2020, ApJ, 889, 45

Szkody P. et al., 2006, AJ, 131, 973

Sánchez B. et al., 2012, in Proc. SPIE Conf. Ser. Vol. 8446, Ground-based and Airborne Instrumentation for Astronomy IV. SPIE, Bellingham, p. 84464T

Tappert C., Gänsicke B. T., Schmidtobreick L., Aungwerojwit A., Mennickent R. E., Koester D., 2007, A&A, 474, 205

Tappert C., Gänsicke B. T., Schmidtobreick L., Ribeiro T., 2011, A&A, 532, A129

Temmink K. D., Toonen S., Zapartas E., Justham S., Gänsicke B. T., 2020, A&A, 636, A31

Tout C. A., Wickramasinghe D. T., Liebert J., Ferrario L., Pringle J. E., 2008, MNRAS, 387, 897

Tremblay P.-E., Bergeron P., Gianninas A., 2011, ApJ, 730, 128

Tremblay P.-E., Cukanovaite E., Gentile Fusillo N. P., Cunningham T., Hollands M. A., 2019, MNRAS, 482, 5222

Tremblay P.-E., Fontaine G., Freytag B., Steiner O., Ludwig H.-G., Steffen M., Wedemeyer S., Brassard P., 2015, ApJ, 812, 19

Tremblay P.-E. et al., 2017, MNRAS, 465, 2849

Tremblay P.-E. et al., 2020, MNRAS, 497, 130

Vanderbosch Z. et al., 2020, ApJ, 897, 171

Vanderburg A. et al., 2015, Nature, 526, 546

van Dokkum P. G., 2001, PASP, 113, 1420

Veras D., Wolszczan A., 2019, MNRAS, 488, 153

Visvanathan N., Wickramasinghe D. T., 1979, Nature, 281, 47

Wegg C., Phinney E. S., 2012, MNRAS, 426, 427

Weisskopf M. C., Wu K., Trimble V., O'Dell S. L., Elsner R. F., Zavlin V. E., Kouveliotou C., 2007, ApJ, 657, 1026

Weiss N. O., 1966, Proceedings of the Royal Society of London Series A, 293, 310

Werner K., 1991, A&A, 251, 147

Werner K., Heber U., Hunger K., 1991, A&A, 244, 437

Wickramasinghe D. T., Farihi J., Tout C. A., Ferrario L., Stancliffe R. J., 2010, MNRAS, 404, 1984

Woelk U., Beuermann K., 1992, A&A, 256, 498

Wright E. L. et al., 2010, AJ, 140, 1868

York D. G. et al., 2000, AJ, 120, 1579

This paper has been typeset from a TEX/LATEX file prepared by the author.